Flow, Turbulence and Combustion **65:** 369–392, 2000.

Maximum Spatial Growth of Görtler Vortices

C. COSSU, J.-M. CHOMAZ, P. HUERRE and M. COSTA
Laboratoire d'Hydrodynamique (LadHyX), CNRS – École Polytechnique, F-91128 Palaiseau Cedex, France

Received 13 December 1999; accepted in revised form 11 July 2000

Abstract. This study is concerned with the numerical calculation of the maximum spatial growth of Görtler vortices on a concave wall. The method is based on the direct computation of a discrete approximation to the spatial propagator that relates the downstream response to the inlet perturbation. The optimization problem is then solved directly by making use of the propagator matrix. The calculated inlet optimal perturbations and the outlet optimal response are similar to those found by Andersson et al. [2] and Luchini [14] in the case of the boundary layer on a flat plate. The only noticeable difference is that the perturbation keeps growing downstream when the wall is curved, whereas the growth is only transient when the wall is flat. The study of a simple "toy" model problem demonstrates that the streamwise evolution of perturbations is essentially determined by the non-normality of the spatial propagator.

Key words: Görtler vortices, boundary layers, non-normality, instability.

1. Introduction

Streamwise periodic counter rotating vortices, called Görtler vortices, are known to grow in boundary layers along a concave wall. For instance, such structures have been observed over the concave part of laminar flow wings and swept wings, on the inner wall of supersonic nozzles, or in turbulent boundary layers over turbomachinery blades. Whereas the centrifugal instability between coaxial cylinders gives rise to Taylor vortices that develop and saturate in time and are homogeneous in space, the centrifugal instability in curved boundary layers gives rise to Görtler vortices that are approximately steady but develop in space. Large amplitude Görtler vortices are subject to secondary instabilities which may lead to transition to turbulence [8, 13, 17, 19]. Quantifying their spatial growth is therefore a necessary preliminary step if one is to arrive at a satisfactory description of the transition process. The objective of the present investigation is twofold. First we want to quantify the maximum streamwise spatial growth that may be experienced by a disturbance between two stations in a concave boundary layer. Second, from the knowledge of the maximum possible growth and of the associated optimal inlet perturbations, we wish to understand the nature of the amplification mechanism.

Stability investigations of curved boundary layers began in 1941 with the pioneering work of Görtler [10] who, building on the analysis for the Taylor problem,

computed the neutral curve by considering the basic flow to be parallel, i.e. homogeneous in the streamwise direction. A consistent set of non-separable partial differential equations for the linear *non-parallel* stability problem, taking into account the growth of the boundary layer, was first obtained by Hall [11, 12] within the limit of high Reynolds numbers and small curvature. This system was originally derived by Floryan and Saric [9] but analyzed by these authors from a *local* point of view, i.e. assuming perturbations in the form of normal modes. Hall [12] has consistently argued that local stability analyses are formally justified only when the boundary layer thickness is large compared to the spanwise wavelength of Görtler vortices. When the boundary layer thickness is of the order of the spanwise wavelength or smaller, which is always the case in some upstream region near the plate leading edge, the full non-separable set of equations has to be integrated by resorting to a downstream marching technique. Since the spatial stability problem is parabolic, the specification of the perturbations at a given upstream station fully determines the disturbance field over the entire flow. The response of the boundary layer, i.e. the streamwise evolution of perturbations along the concave wall, is then very sensitive to inlet conditions [12]. This brought Saric [19] to state that the dependence of the streamwise development on inlet conditions is so strong that "somewhat universal charts ... of use to the designer or someone who is unwilling to do the calculations" are not yet available. Even if different upstream perturbations are examined, one cannot be sure to have identified the most "dangerous" conditions, i.e. the ones which produce the largest amplitude at a particular downstream location: searching for the "optimal" upstream perturbations might require an infinite number of simulations.

In the present article, an optimization technique is implemented to evaluate the most dangerous inlet conditions associated with the largest spatial growth for each downstream station. The technique, which relies on the definition of a spatial "propagator" [7], is inspired by the methodologies used to evaluate optimal perturbations in temporal stability problems. The temporal propagator for the evolution of perturbations is here replaced by its spatial counterpart.

The linear receptivity of Görtler vortices to wall roughness and to free-stream disturbances impinging the boundary layer at the leading edge, has recently been addressed by Luchini and Bottaro [15]. Their method consists in the upstream integration of the adjoint linear stability equations from sufficiently far downstream, in order to determine the "optimal", i.e. most spatially amplified, inlet conditions. Optimal perturbations maximizing spatial transient growth have been evaluated by Lundbladh et al. [16] for plane Poiseuille flow and the Blasius boundary layer, assuming in the latter instance the basic flow to be parallel. In the fully non-parallel case, Andersson et al. [2] and Luchini [14] have recently investigated the maximum transient growth and associated optimal perturbations at the leading edge of the Blasius boundary layer on a flat plate by resorting to an iterative upstream-downstream marching procedure.

The methodological point of view taken in the present study consists in choosing an inlet station, for given values of the Görtler number and spanwise wavelength, and in computing, as a function of downstream distance, the most dangerous inlet conditions which maximize the gain, i.e. the growth in amplitude, between the inlet and some downstream station. This is made possible by the use of a "flexible" technique based on the post-processing of numerically computed downstream evolutions from a complete set of linearly independent upstream perturbations. The method relies on a consistent discrete approximation, expressed in matrix form, of the spatial propagator; the discrete adjoint propagator is simply obtained by transposing the propagator matrix. The approach is not limited to parabolic systems of equations since it does not necessitate marching integrations. It remains applicable to the full Navier–Stokes equations. As the optimization procedure is decoupled from the evaluation of the propagator, different metrics may be computed at will.

The standard mathematical formulation of the Görtler instability problem is recalled in Section 2 together with the basic optimization concepts, namely the notions of gain curve, maximum gain curve and spatial propagator. The numerical procedure, discussed in Section 3, allows us to determine the maximum gain experienced by the perturbations between an inlet station x_0 and an optimization station x. The physical implication of the numerically obtained results are discussed in Section 4. A simple "toy" model is proposed in Section 5 to account for the sensitivity of the amplitude of the downstream response to different inlet conditions. The main conclusions are summarized and discussed in connection with recent related investigations in Section 6.

2. Mathematical Formulation

2.1. DISTURBANCE EQUATIONS

The linear stability analysis is based on the non-separable set of partial differential equations derived by Hall [11, 12]. Consider the Blasius boundary layer, with external velocity U_∞^* in an incompressible fluid of kinematic viscosity ν^* and density ρ^*, over a wall of radius of curvature $\mathcal{R}^*$ large compared to the boundary layer thickness. The analysis is limited to stationary disturbances, periodic in the spanwise direction z^* of wavenumber β^*. Given a typical streamwise reference length L^*, the Reynolds and Görtler numbers are defined as:

$$\mathrm{Re} = U_\infty^* L^* / \nu^*, \tag{1}$$

$$\mathrm{G}^2 = \mathrm{Re}^{1/2}(L^*/\mathcal{R}^*). \tag{2}$$

The streamwise coordinate along the wall is denoted by x^*, the coordinate normal to the wall by y^*. The streamwise, normal and spanwise velocity components are denoted respectively by u^*, v^*, w^*, the pressure by p^*. Following the Prandtl scaling for the boundary layer, we rescale x^* by L^*, y^* and z^* by a length $\mathrm{Re}^{-1/2}L^*$

which is proportional to the boundary layer thickness at the streamwise location L^*, u^* by U_∞^*, v^* and w^* by $\mathrm{Re}^{-1/2}U_\infty^*$; finally, p^* is made dimensionless with respect to $\rho^* U_\infty^{*2}$. The asterisk is dropped for dimensionless variables. The Blasius self-similar solution for the two-dimensional base flow is denoted by $U(x, y)$, $V(x, y)$. Three-dimensional perturbations to the base flow are assumed to be periodic in the streamwise direction of the form

$$u(x, y)\cos(\beta z), \quad v(x, y)\cos(\beta z), \quad w(x, y)\sin(\beta z), \quad p(x, y)\cos(\beta z), \tag{3}$$

where $\beta \equiv \beta^* \mathrm{Re}^{-1/2} L^*$ is the nondimensional spanwise wavenumber. Upon assuming that $\mathrm{Re} \gg 1$, $(\mathcal{R}^*/L^*) \gg 1$ and $G = O(1)$, we obtain, at leading order, the linear partial differential equations derived by Hall [11, 12] and Floryan and Saric [9]:

$$\frac{\partial u}{\partial x} + \frac{\partial v}{\partial y} + \beta w = 0, \tag{4}$$

$$U\frac{\partial u}{\partial x} + V\frac{\partial u}{\partial y} + \frac{\partial U}{\partial x}u + \frac{\partial U}{\partial y}v - \frac{\partial^2 u}{\partial y^2} + \beta^2 u = 0, \tag{5}$$

$$U\frac{\partial v}{\partial x} + V\frac{\partial v}{\partial y} + \frac{\partial V}{\partial x}u + \frac{\partial V}{\partial y}v - \frac{\partial^2 v}{\partial y^2} + \beta^2 v + \frac{\partial p}{\partial y} + 2G^2 U u = 0, \tag{6}$$

$$U\frac{\partial w}{\partial x} + V\frac{\partial w}{\partial y} - \frac{\partial^2 w}{\partial y^2} + \beta^2 w - \beta p = 0. \tag{7}$$

Elimination of the pressure and of the spanwise component of the velocity w, yields the following system [12]:

$$M^{(uu)}\frac{\partial u}{\partial x} + M^{(uv)}\frac{\partial v}{\partial x} + L^{(uu)}u + L^{(uv)}v = 0, \tag{8}$$

$$M^{(vu)}\frac{\partial u}{\partial x} + M^{(vv)}\frac{\partial v}{\partial x} + L^{(vu)}u + L^{(vv)}v = 0, \tag{9}$$

where x-derivatives have been explicitly isolated. The linear differential operators $M^{(ab)}$ and $L^{(ab)}$ and the associated boundary conditions for the perturbations, which solely involve the base flow and its derivatives with respect to y, are specified in Appendix A. From the continuity equation (4), the spanwise velocity component w can be expressed as a function of u and v in the form

$$\beta w = -\left(M^{(uu)}\right)^{-1} L^{(uu)}u - \left[\left(M^{(uu)}\right)^{-1} L^{(uv)} + \frac{\partial}{\partial y}\right]v. \tag{10}$$

As remarked by Hall [12], system (8–9) is parabolic in the streamwise variable x and can be solved as an initial value problem in x once suitable initial conditions at x_0, also called upstream forcing or "inlet conditions", have been specified:

$$u(x_0, y) = u_{[x_0]}(y), \quad v(x_0, y) = v_{[x_0]}(y). \tag{11}$$

The *state vector* $s_{[x]}(y)$ at the streamwise station x is composed of the two velocity components $\{u(x, y), v(x, y)\}$. Note that x being the evolution variable, $s_{[x]}(y)$ is considered as a function of y with x appearing as a parameter. The inlet condition on the state vector is denoted by $s_{[x_0]}(y) \equiv \{u(x_0, y), v(x_0, y)\}$.

2.2. SPATIAL GROWTH OPTIMIZATION

To quantify the downstream growth of perturbations, the gain g at the location x is defined as the ratio of the disturbance outlet magnitude at location x to its inlet magnitude at location x_0:

$$g(x_0, s_{[x_0]}, x) = \|s_{[x]}\|_{\text{out}} / \|s_{[x_0]}\|_{\text{in}}. \tag{12}$$

The inlet measure $\|\cdot\|_{\text{in}}$ may in all generality differ from the outlet measure $\|\cdot\|_{\text{out}}$. The gain also depends on the particular perturbation $s_{[x_0]}$ applied at the inlet as well as on the inlet and outlet locations x_0 and x. The optimization problem considered here is the following: given an inlet location x_0, a Görtler number G and spanwise wavenumber β, determine, for every "observation" station x, the inlet condition $s_{[x_0]}$ that produces the maximum possible gain between x_0 and x

$$\mathcal{G}(x_0, x) = \sup_{s_{[x_0]} \neq 0} g(x_0, s_{[x_0]}, x). \tag{13}$$

The maximum gain curve $\mathcal{G}(x_0, x)$ is therefore the least upper bound of the outlet magnitudes $\|s_{[x]}\|_{\text{out}}$ to all possible inlet conditions $s_{[x_0]}$ say of inlet norm unity $\|s_{[x_0]}\|_{\text{in}} = 1$.

Since the problem is parabolic, the response $s_{[x]}(y)$ at x, to the inlet condition $s_{[x_0]}(y)$ enforced at x_0, is formally given by

$$s_{[x]} = P_{[x,x_0]} s_{[x_0]}, \tag{14}$$

where $P_{[x,x_0]}$ is a linear operator called the *spatial propagator*. This operator maps the inlet condition $s_{[x_0]}(y)$ applied at x_0, to the outlet condition $s_{[x]}(y)$ at location x, and it is such that $P_{[x_0,x_0]} = I$, where I is the identity operator. This definition is inspired by the theory of non-autonomous systems of ordinary differential equations [5] and it is analogous to the definition of the temporal propagator introduced by Farrell and Ioannou [7] in the context of generalized *temporal* stability theory.

If definition (14) is substituted into Equation (13) one finds that

$$\mathcal{G}(x_0, x) = \sup_{s_{[x_0]} \neq 0} \frac{\|P_{[x,x_0]} s_{[x_0]}\|_{\text{out}}}{\|s_{[x_0]}\|_{\text{in}}}. \tag{15}$$

The evaluation of the maximum spatial growth therefore reduces to an optimization problem for the spatial propagator $P_{[x,x_0]}$. The optimization depends on the definition of the input and output disturbance measures. The inlet condition which realizes the maximum gain between x_0 and the "observation" station x is referred to as the $x_0 - x$ *optimal inlet condition.*

2.3. GROWTH MEASURES

The velocity components u, v, and w considered so far have been scaled according to the classical Prandtl boundary layer definitions. The most natural disturbance measure is probably the "physical" perturbation energy with respect to unscaled velocity variables as introduced by Andersson et al. [2]. In that case v and w must be multiplied by $\mathrm{Re}^{-1/2}$ in order to recover their unscaled value. The "physical" perturbation energy is a norm which may be used to define a gain

$$g_{\mathrm{A}}^2(x_0, s_{[x_0]}, x) = \frac{\int_0^\infty \left[u_{[x]}^2 + \mathrm{Re}^{-1}(v_{[x]}^2 + w_{[x]}^2)\right] \mathrm{d}y}{\int_0^\infty \left[u_{[x_0]}^2 + \mathrm{Re}^{-1}(v_{[x_0]}^2 + w_{[x_0]}^2)\right] \mathrm{d}y}, \tag{16}$$

where the subscript "A" stands for Andersson et al. [2]. Both the maximum spatial growth and the optimal perturbations then seem to depend on the Reynolds number. Since the Blasius solution is asymptotically valid in the limit $\mathrm{Re} \gg 1$, Luchini [14] observed that in that limit, the energy at the outlet is given by the streamwise velocity component u only and that the minimum inlet energy is obtained when $u_{[x_0]} \equiv 0$. Luchini therefore proposed to consider instead the leading order (Re^{-1}) spatial gain defined by:

$$g_{\mathrm{L}}^2(x_0, v_{[x_0]}, x) = \mathrm{Re} \frac{\int_0^\infty u_{[x]}^2 \, \mathrm{d}y}{\int_0^\infty (v_{[x_0]}^2 + w_{[x_0]}^2) \, \mathrm{d}y}, \quad u_{[x_0]} = 0, \tag{17}$$

where the subscript "L" stand for Luchini [14]. The maximum spatial growth is then

$$\mathcal{G}_{\mathrm{L}}^2(x_0, x) = \mathrm{Re} \sup_{v_{[x_0]} \neq 0, u_{[x_0]} = 0} \frac{\int_0^\infty u_{[x]}^2 \, \mathrm{d}y}{\int_0^\infty (v_{[x_0]}^2 + w_{[x_0]}^2) \, \mathrm{d}y}. \tag{18}$$

In this case, the optimal perturbations do not depend on the Reynolds number, as the Reynolds number does not enter the optimization process, and the maximum spatial growth $\mathcal{G}_{\mathrm{L}}(x_0, x)$ scales linearly with the square root of the Reynolds number.

The numerical method implemented in the present study separates the computation of the spatial propagator from the optimization process. It therefore allows to compute the optimal inlet perturbations and maximum spatial growths by a simple postprocessing. In the following maximum spatial growths and optimal perturbations are evaluated for the Luchini gain g_{L}.

3. Numerical Method

3.1. DISCRETIZATION PROCEDURE

The downstream marching procedure proposed by Hall [12] is used to numerically solve the parabolic system given by Equations (8), (9) under the inlet condition (11). The linear stability equations are rewritten in boundary layer similarity variables (x, η) with $\eta = y/(2x^{1/2})$ and discretized on a uniform grid

$$\begin{aligned} x_k &= x_0 + k\Delta x, \quad k = 0, \ldots, N_x; \\ \eta_j &= j\Delta\eta, \quad j = 0, \ldots, N_\eta. \end{aligned} \tag{19}$$

At the kth streamwise station x_k we denote by $\mathbf{u}_{[x_k]}$ the vector formed by the $N_\eta - 1$ values $u(\eta_j)$ of the u-velocity component at the cross-stream stations η_j, $j = 1, \ldots, N_\eta - 1$. The values for $j = 0$ and $j = N_\eta$ are known from the boundary conditions. The vectors $\mathbf{v}_{[x_k]}$ and $\mathbf{w}_{[x_k]}$ are similarly defined with respect to the v- and w-velocity components. As a result of the parabolic nature of the governing equations (8) and (9), it is possible to compute the vectors $\mathbf{u}_{[x_{k+1}]}$ and $\mathbf{v}_{[x_{k+1}]}$ solely from the knowledge of the vectors $\mathbf{u}_{[x_k]}$ and $\mathbf{v}_{[x_k]}$ by a semi-implicit downstream marching procedure. The process is initiated at station x_0 where the inlet condition (11) is specified. The reader is referred to Hall [12] for details of the numerical method which is second order accurate in η and first order accurate in x. The streamwise step used to numerically march downstream is $\Delta x = 0.1$. The free-stream boundary conditions are enforced at $\eta_{N_\eta} = 20$ or $\eta_{N_\eta} = 35$ (to minimize finite box effects) and the number N_η of points in the normal direction ranges from 200 to 350 so as to keep the cross-stream mesh spacing $\Delta\eta$ close to 0.1.

3.2. DETERMINATION OF THE DISCRETE PROPAGATOR

Let $\mathbf{s}_{[x_k]}$ denote the state vector at the location x_k, constructed with the $N_\eta - 1$ discretized values of the u-profile and the $N_\eta - 1$ values of the v-profile:

$$\mathbf{s}_{[x_k]} = \begin{Bmatrix} \mathbf{u}_{[x_k]} \\ \mathbf{v}_{[x_k]} \end{Bmatrix}. \tag{20}$$

The discrete propagator $\mathbf{P}_{[x_k,x_0]}$, associated with the discrete system, is formally defined by the relation

$$\mathbf{s}_{[x_k]} = \mathbf{P}_{[x_k,x_0]}\mathbf{s}_{[x_0]}. \tag{21}$$

The above matrix relation is the discrete counterpart of the continuous equation (14) defining the spatial propagator $P_{[x,x_0]}$. The $2(N_\eta - 1) \times 2(N_\eta - 1)$ matrix $\mathbf{P}_{[x_k,x_0]}$ effectively specifies a linear mapping between the discrete inlet condition $\mathbf{s}_{[x_0]}$ at the grid point x_0 and the discrete outlet response $\mathbf{s}_{[x_k]}$ at the grid point x_k. As for non-autonomous systems of ordinary differential equations [5], it is convenient

to introduce the $2(N_\eta - 1) \times 2(N_\eta - 1)$ fundamental matrix $\mathbf{\Phi}_{[x_k]}$ of the discrete system constructed as follows: $2(N_\eta - 1)$ linearly independent inlet conditions $\mathbf{s}^{(i)}_{[x_0]}$, $i = 1, \ldots, 2(N_\eta - 1)$, are selected and their evolution $\mathbf{s}^{(i)}_{[x_k]}$ is numerically determined. The ith column of $\mathbf{\Phi}_{[x_k]}$ is then the $2(N_\eta - 1)$ vector $\mathbf{s}^{(i)}_{[x_k]}$. As each column of $\mathbf{\Phi}_{[x_k]}$ satisfies Equation (21), the fundamental matrix satisfies a tensor equation formally similar to (21):

$$\mathbf{\Phi}_{[x_k]} = \mathbf{P}_{[x_k,x_0]}\mathbf{\Phi}_{[x_0]}. \tag{22}$$

Once $\mathbf{\Phi}_{[x_0]}$ and $\mathbf{\Phi}_{[x_k]}$ are known, the discrete propagator may readily be retrieved from (22) via the relation

$$\mathbf{P}_{[x_k,x_0]} = \mathbf{\Phi}_{[x_k]}\mathbf{\Phi}^{-1}_{[x_0]}. \tag{23}$$

In the present investigation, the inlet fundamental matrix has been chosen so that $\mathbf{\Phi}_{[x_0]} = \mathbf{I}$, whereby Equation (23) reduces to $\mathbf{P}_{[x_k,x_0]} = \mathbf{\Phi}_{[x_k]}$: the fundamental matrix at x_k simply coincides with the discrete propagator $\mathbf{P}_{[x_k,x_0]}$.

In practice $\mathbf{\Phi}_{[x_0]} = \mathbf{I}$ corresponds to the set of initial conditions such that either the u- or v-velocity component is non-zero at a single grid point in η. Every inlet condition that may be considered in a numerical simulation can be expressed as a linear combination of the above defined independent inlet conditions. Of course other choices for the complete basis that spans the space of inlet conditions would also be adequate for the present analysis.

3.3. SPATIAL GROWTH OPTIMIZATION

The discretization of the gain g_L between the inlet station x_0 and the outlet station x is detailed in Appendix B. The discrete counterpart of g_L defined in (17), is given by Equation (51), i.e.

$$g_L^2(x_0, \mathbf{v}_{[x_0]}, x_k)/\mathrm{Re} = \left(\frac{x_k}{x_0}\right)^{1/2} \frac{\mathbf{u}^T_{[x_k]}\mathbf{u}_{[x_k]}}{\mathbf{v}^T_{[x_0]}\mathbf{v}_{[x_0]} + \mathbf{w}^T_{[x_0]}\mathbf{w}_{[x_0]}}, \tag{24}$$

where the T superscript indicates the transpose and it has been assumed that $\mathbf{u}_{[x_0]} \equiv \mathbf{0}$. The term $(x_k/x_0)^{1/2}$ in (24) is a rescaling factor due to the fact that the mesh is fixed in the η similarity variable whereas the integrals in (17) are performed with respect to y. Equation (21) may more explicitly be written as

$$\begin{Bmatrix} \mathbf{u}_{[x_k]} \\ \mathbf{v}_{[x_k]} \end{Bmatrix} = \begin{bmatrix} \mathbf{P}^{(uu)}_{[x_k,x_0]} & \mathbf{P}^{(uv)}_{[x_k,x_0]} \\ \mathbf{P}^{(vu)}_{[x_k,x_0]} & \mathbf{P}^{(vv)}_{[x_k,x_0]} \end{bmatrix} \begin{Bmatrix} \mathbf{u}_{[x_0]} \\ \mathbf{v}_{[x_0]} \end{Bmatrix}, \tag{25}$$

with a straightforward definition for the various submatrices $\mathbf{P}^{(uu)}_{[x_k,x_0]}$, ... The discrete counterpart of Equation (10) similarly reads

$$\mathbf{w}_{[x_0]} = \begin{bmatrix} \mathbf{Q}^{(wu)}_{[x_0]} & \mathbf{Q}^{(wv)}_{[x_0]} \end{bmatrix} \begin{Bmatrix} \mathbf{u}_{[x_0]} \\ \mathbf{v}_{[x_0]} \end{Bmatrix}. \tag{26}$$

By substitution of (25) and (26) into (24) and bearing in mind that $\mathbf{u}_{[x_0]} = \mathbf{0}$, it is found that

$$g_L^2(x_0, \mathbf{v}_{[x_0]}, x_k)/\mathrm{Re} = \left(\frac{x_k}{x_0}\right)^{1/2} \frac{\mathbf{v}_{[x_0]}^T \mathbf{P}_{[x_k,x_0]}^{(uv)\,T} \mathbf{P}_{[x_k,x_0]}^{(uv)} \mathbf{v}_{[x_0]}}{\mathbf{v}_{[x_0]}^T \left[\mathbf{I} + \mathbf{Q}_{[x_0]}^{(wv)\,T} \mathbf{Q}_{[x_0]}^{(wv)}\right] \mathbf{v}_{[x_0]}}. \tag{27}$$

The maximum gain $\mathcal{G}_L$ defined in Equation (18), is obtained by maximizing over all possible inlet cross-stream velocities $\mathbf{v}_{[x_0]} \neq \mathbf{0}$ the r.h.s. of Equation (27). The maximum is obtained [2, 14, 24] by finding the largest eigenvalue $\lambda_L^{(opt)}$ of the generalized eigenvalue problem

$$\left[\mathbf{P}_{[x_k,x_0]}^{(uv)\,T} \mathbf{P}_{[x_k,x_0]}^{(uv)}\right] \mathbf{v}_{[x_0]} = \lambda \left[\mathbf{I} + \mathbf{Q}_{[x_0]}^{(wv)\,T} \mathbf{Q}_{[x_0]}^{(wv)}\right] \mathbf{v}_{[x_0]}. \tag{28}$$

The numerically evaluated maximum gain is then given by

$$\mathcal{G}_L^2(x_0, x_k)/\mathrm{Re} = (x_k/x_0)^{1/2} \lambda_L^{(\mathrm{opt})}, \tag{29}$$

and the corresponding eigenvector $\mathbf{v}_{[x_0]}^{(\mathrm{opt})}$ is the v-optimal perturbation. The w-optimal perturbation is deduced from Equation (26): since $\mathbf{u}_{[x_0]} \equiv \mathbf{0}$, $\mathbf{w}_{[x_0]}^{(\mathrm{opt})} = \mathbf{Q}_{[x_0]}^{(wv)} \mathbf{v}_{[x_0]}^{(\mathrm{opt})}$. Both LAPACK routines [1] and the power iterations method [18] have been used in order to numerically determine $\lambda_L^{(\mathrm{opt})}$ and $\mathbf{v}_{[x_0]}^{(\mathrm{opt})}$.

In Appendix C we briefly compare the computational cost of the direct approach used here to the iterative direct-adjoint approach used by Andersson et al. [2] and Luchini [14].

4. Optimal Inlet Conditions and Maximum Growth

The numerical results shown in the following pertain to the Görtler number $G = 0.224$ and the spanwise wavenumber $\beta = 0.069$ considered by Hall [12]. In order to compare results based on different reference lengths L^* it is customary to define a Görtler number based on the local streamwise position $\mathrm{G}_x^2 = \mathrm{Re}_x^{1/2}(x^*/\mathcal{R}^*)$ (with $\mathrm{Re}_x = x^* U_\infty^*/\nu_*$)and spanwise wavelength parameter $\Lambda \equiv (U_\infty^* \lambda^*/\nu^*)(\lambda^*/\mathcal{R}^*)^{1/2}$. The followings relations hold: $\mathrm{G}_x = \mathrm{G}x^{3/4}$, $\Lambda = G(2\pi/\beta)^{3/2}$. For the values of G and β specified above, $\Lambda = 97.5$. The correspondence between the x values used in the following and the corresponding G_x is given in Table I.

Since the boundary layer thickness $\delta(x)$ increases as $x^{1/2}$, the ratio of the spanwise wavelength λ to $\delta(x)$ decreases both in dimensional and dimensionless variables (recall that both the wavelength and the normal coordinate were rescaled with respect to the same reference length $\mathrm{Re}^{-1/2} L^*$). For instance, for the considered wavenumber, the wavelength of the Görtler vortices is almost four times the boundary layer thickness $\delta(x)$ at $x = 10$, twice $\delta(x)$ at $x = 40$ and decreases to less than $\delta(x)$ at $x = 165$ (the boundary layer thickness is where

Table I. Correspondence between the values of the abscissa x most used in the present study and the corresponding G_x values (for $G = 0.224$).

x	G_x
20	2.128
40	3.56
120	8.12
200	11.91
240	13.65

the streamwise component of the base velocity is 99% of the free-stream velocity [20]). In the upstream region where the wavelength is larger than the boundary layer thickness and where the boundary layer thickness varies rapidly, the local weakly non-parallel approach does not apply [12]. Further downstream, say for $x > 165$, the wavelength becomes smaller than the boundary layer thickness and $\delta(x)$ varies slowly, so that the local normal mode decomposition should apply and the response to any inlet perturbation should converge to the most amplified mode of the local theory, as pointed out by Hall [11–13], Day et al. [6] and Bottaro and Luchini [4]. In particular, the latter authors have used a second-order development in G_x^{-1} to extend the range of applicability of local normal mode theory to larger spanwise wavelengths than in earlier investigations.

Figure 1a displays, in the z–η plane, the optimal inlet perturbation vector field $w_{[x_0]}^{(\mathrm{opt})}$-$v_{[x_0]}^{(\mathrm{opt})}$ which maximizes the g_L gain between the inlet location $x_0 = 20$ and $x = 200$. This inlet perturbation produces at the streamwise station $x = 240$, considered by Hall [12], the u-field plotted in Figure 1b. Since $u_{[x_0]} \equiv 0$, the optimal inlet condition consists of periodic streamwise vortex pairs (Figure 1a) which develops into periodic streamwise streaks with $u_{[x_0]} \neq 0$ (Figure 1b). These streaks are alternating regions of high and low streamwise velocity u that may strongly deform the Blasius velocity field, thereby leading to locally inflectional velocity profiles [22]. The optimization of the g_L gain yields the purely streamwise vortices of norm unity which are the most efficient in producing large-amplitude streaks.

The effect of the optimization station x on the optimal inlet perturbation is considered in Figure 2, where three different optimal inlet conditions at $x_0 = 20$ are shown that maximize the gain $g_L(x_0, v_{[x_0]}, x)$ respectively at (a) $x = 40$, (b) $x = 120$ and (c) $x = 200$. Recall that in the definition of the g_L gain $u_{[x_0]} = 0$. In the figure, $v_{[x_0]}^{(\mathrm{opt})}(\eta)$ and $w_{[x_0]}^{(\mathrm{opt})}(\eta)$ are normalized so that $\int_0^\infty (v_{[x_0]}^2 + w_{[x_0]}^2)\, \mathrm{d}\eta = 1$. All optimal perturbations are seen to have a similar structure: a v-component with one extremum and a w-component with two extrema of opposite sign. Optimal

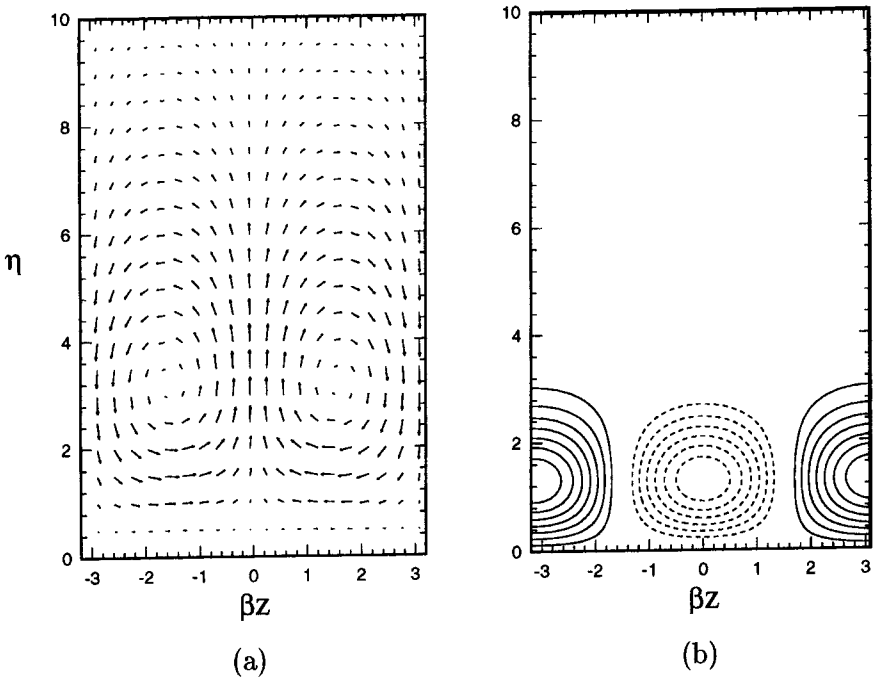

Figure 1. View in the z–η plane of the transverse $w_{[x_0]} - v_{[x_0]}$ velocity field associated with optimal inlet conditions (a) and magnitude of the corresponding streamwise u-velocity component generated at $x = 240$ (b) for the Luchini gain. The displayed optimal velocity field corresponds to case (c) of Figures 2 and 3, i.e. optimal inlet conditions (a) are applied at $x_0 = 20$ and the gain is maximized at $x = 200$, while their evolution (b) is shown at $x = 240$.

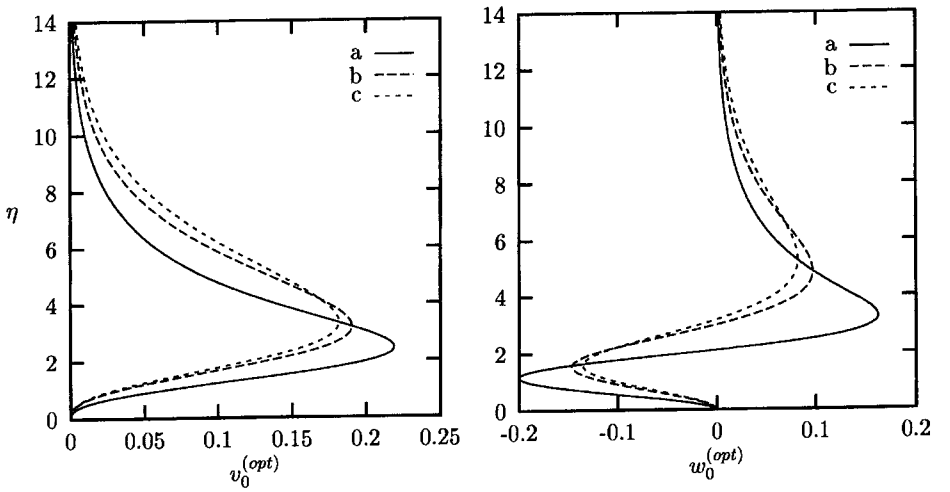

Figure 2. Optimal inlet conditions applied at $x_0 = 20$ which maximize the g_L gain respectively at (a) $x = 40$, (b) $x = 120$, (c) $x = 200$. Left: normal distribution of normal perturbation velocity $v_{[x_0]}(\eta)$. Right: normal distribution of spanwise perturbation velocity $w_{[x_0]}(\eta)$. The curves corresponding to cases (b) and (c) nearly coincide.

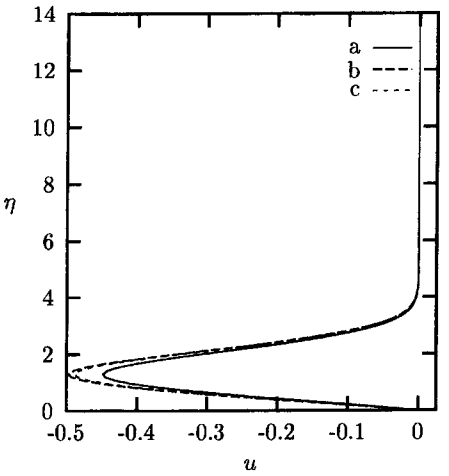

Figure 3. u-perturbation velocity profiles at $x = 240$, for inlet conditions (a), (b) and (c) of Figure 2.

perturbations for the location $x = 200$ correspond to the vortices represented in Figure 1a. As the optimization location x moves downstream, these vortices gradually move away from the wall (Figure 2) and the v- and w-optimal perturbations at the inlet $x_0 = 20$ appear to converge asymptotically to the same form.

The u-velocity profiles produced at the downstream location $x = 240$ by the three inlet perturbations in Figure 2 are represented in Figure 3. The u-velocity profiles are seen to differ in amplitude but not in shape. Solutions (b) and (c), optimal at $x = 120$ and $x = 200$ respectively, are nearly undistinguishable at $x = 240$ whereas solution (a), optimal at $x = 40$, remains of slightly lower amplitude. As already mentioned, this convergence of the downstream velocity field to a unique shape may be attributed to the emergence of a most amplified downstream mode given by local theory.

The maximum gain curve $\mathcal{G}_L(x_0, x)$ and the individual gain curves $g_L(x_0, \mathbf{v}_{[x_0]}, x)$ corresponding to the different inlet conditions specified in Figure 2 are represented on a semi-log plot in Figure 4. The gain curves associated with inlet conditions (a), (b) and (c) that maximize the gain respectively at $x = 40$, 120 and 200 are seen to be tangent to the maximum gain curve $\mathcal{G}_L(x_0, x)$ at these stations as required by definition (13). The gain curves associated with optimal inlet conditions (b) and (c) almost coincide with the maximum gain curve $\mathcal{G}_L(x_0, x)$ over an extended streamwise range. As already noticed in the context of Figure 2, whenever the optimization station is moved sufficiently far downstream from the inlet station x_0, the response and thus the gain curves $g_L(x_0, \mathbf{v}_{[x_0]}, x)$ become nearly insensitive to the optimization station.

In order to investigate the effect of the inlet location x_0, computations have been performed for the single fixed optimization station $x = 200$ and different inlet stations x_0. The v- and w-optimal inlet conditions pertaining to (d) $x_0 = 10$,

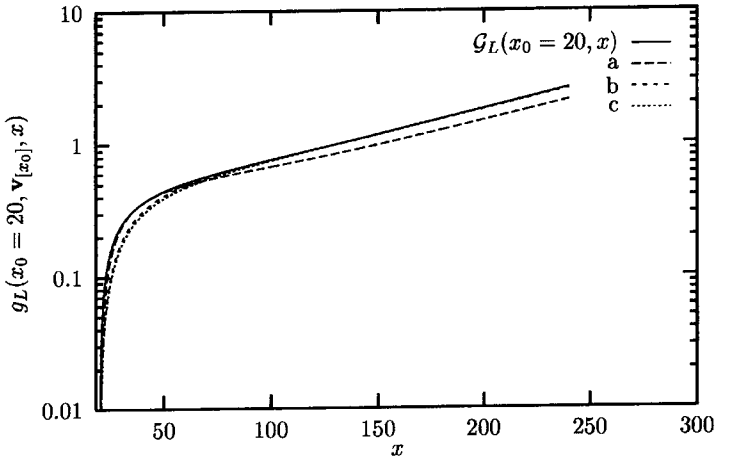

Figure 4. Gain curves $g_L(x_0, \mathbf{v}_{[x_0]}, x)/\mathrm{Re}^{1/2}$ associated with inlet conditions (a), (b) and (c) of Figure 2. The maximum gain curve $\mathcal{G}_L(x_0, x)/\mathrm{Re}^{1/2}$ is indicated by a continuous bold line located above all the curves $g_L(x_0, \mathbf{v}_{[x_0]}, x)/\mathrm{Re}^{1/2}$.

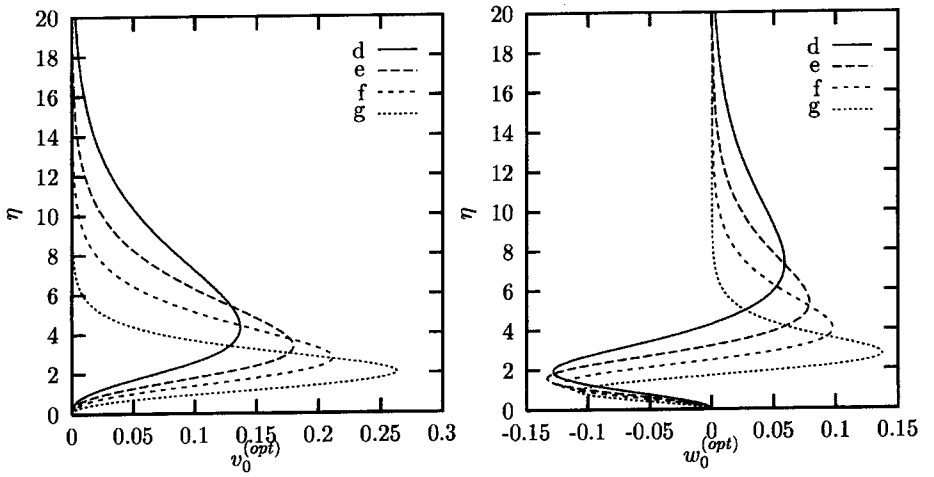

Figure 5. Optimal perturbations with varying inlet station. Left: normal distribution of normal perturbation velocity $v_{[x_0]}(\eta)$. Right: cross-stream distribution of spanwise perturbation velocity $w_{[x_0]}(\eta)$ that optimize the gain at $x = 200$ for (d) $x_0 = 10$, (e) $x_0 = 20$, (f) $x_0 = 40$, (g) $x_0 = 120$.

(e) $x_0 = 20$, (f) $x_0 = 40$, (g) $x_0 = 120$ are shown in Figure 5 as a function of the similarity variable η. The v- and w-optimal inlet perturbations are observed to become localized further and further away from the wall, outside the boundary layer, as the inlet station x_0 moves closer to the leading edge. This feature demonstrates that the receptivity of the boundary layer changes with inlet location: when the inlet station moves closer to the leading edge, optimal perturbations

Table II. Elevation above the plate of the maximum of the perturbation velocity $v^{(opt)}_{[x_0]}$ optimal at $x = 200$, as a function of x_0/x. The position of the maximum is indicated both in terms of the similarity variable η and in terms of the ratio of the non-rescaled variable y to the spanwise wavelength λ.

x_0/x	η	y/λ
0.6	1.91	0.325
0.2	2.74	0.270
0.1	3.35	0.233
0.05	4.29	0.210

are localized in the free-stream, outside the boundary layer. As the inlet station moves downstream, optimal perturbations become localized within the boundary layer. Surprisingly this shift is slow and at $x_0 = 20$ optimal perturbations are still largely localized outside the boundary layer. This trend is clearly observable in Table II where the elevation η above the plate of the maximum of the v-optimal inlet perturbation (Figure 2) is specified in the second column versus the ratio x_0/x between the inlet and the optimization station (first column). The location η of the maximum increases continuously as x_0/x goes to zero. Also indicated in Table II are the same data given in terms of the original variable y scaled with respect to the spanwise wavelength $\lambda = 2\pi/\beta$. The scaled elevation y/λ of the maximum seems to converge as x_0/x goes to zero, thereby implying that the optimal perturbation converges to a limiting form centered about a finite y/λ elevation as the inlet station x_0 approaches the leading edge $x_0 = 0$. The limitations imposed by the numerical scheme have not enabled us to fully confirm this trend. As x_0 moves closer to zero, the boundary layer thickness decreases while the optimal perturbation moves outside the boundary layer. In order to capture both these phenomena the numerical resolution must concurrently increase over a wider and wider domain. A conservative numerical formulation in x, y variables, similar to the one used by Andersson et al. [2], and Luchini and Bottaro [15] would probably succeed in relaxing this limitation. It is however clear that there is a progressive shift from receptivity to free-stream perturbations to receptivity to boundary layer perturbations as the inlet station gradually moves downstream of the leading edge.

The maximum gain $\mathcal{G}_L$ that may be achieved between different inlet stations x_0 and the fixed downstream outlet station $x = 200$, is displayed in Figure 6. The convergence to a finite value as x_0 moves closer to the leading edge is evident. Moreover for the single spanwise wavelength tested $\beta = 0.069$, the maximum gain slightly decreases between $x_0 = 20$ and $x_0 = 10$, thereby indicating that perturbations upstream of $x_0 = 20$ do not lead to an increase of the downstream perturbation energy. In weakly non-parallel flows the neutral point is usually de-

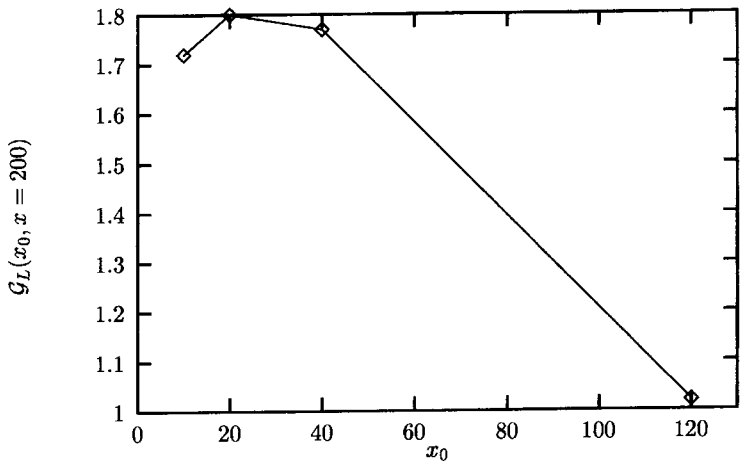

Figure 6. Maximum gain $\mathcal{G}_L(x_0, x = 200)/\mathrm{Re}^{1/2}$, associated with inlet conditions (d), (e), ... (h) of Figure 5.

fined as the streamwise station separating a stable region, where the spatial growth rate of the disturbances is negative, from a region where it is positive. In that case the neutral point is also the most effective inlet station in order to produce the most amplified downstream response. In the present case the definition of a neutral point using a sort of "local" spatial growth rate is meaningless. However, the station $x_0 = 20$, which seems to be the optimal inlet station for the parameter setting used here, could be interpreted as the analogue of a neutral point for the strongly non-parallel problem.

It is striking to note that the present optimal inlet conditions pertaining to the Görtler instability (Figures 1a and 2) display a strong qualitative similarity with the optimal inlet conditions found by Andersson et al. [2] and Luchini [14] in the case of a *flat* plate boundary layer ($G = 0$, i.e. without the centrifugal instability arising from the curvature). The global sensitivity to perturbations and the structure of the response seem to be similar for the flat and the curved boundary layer in spite of distinct local instability properties. Indeed, in the spatial range considered by Andersson et al. [2] and Luchini [14], the flat plate boundary layer is everywhere locally stable while the boundary layer on a concave wall considered here is locally unstable. In the curved plate case, the streaks produced downstream emerge from an instability, whereas in the flat plate boundary layer case, they arise from transient spatial growth. In both cases however they may lead to transition. This resemblance further supports the fact that locally parallel or weakly non-parallel analyses may be misleading in determining the spatial growth of disturbances in the upstream portion of boundary layers. Luchini and Bottaro [15] have computed the optimal free-stream perturbations for the Görtler problem by choosing a metric which is different from the present one: in their case, the inlet disturbance amplitude is measured by its streamwise vorticity (roll receptivity) or by its streamwise velocity

(streak receptivity), so that the present optimal perturbations cannot be directly compared with theirs.

In earlier studies [2, 14, 15] the optimal perturbations were evaluated at the leading edge of the plate ($x_0 = 0$), where the boundary layer has zero thickness, while the optimal perturbations considered here are applied at a streamwise station where the boundary layer has a finite thickness ($x_0 > 0$). At the leading edge the optimal perturbations must be considered as free-stream perturbations, while if the inlet station is sufficiently far downstream the optimal perturbations are internal to the boundary layer. According to the present analysis it is clear that, inbetween these two cases, optimal perturbations are a mix of external and internal disturbances.

5. Non-Normality of the Spatial Propagator

The consistent asymptotic analyses of Hall [11, 12] have clearly emphasized the essential role played by non-parallel effects in the streamwise development of Görtler vortices. It is the purpose of this section to demonstrate that the main features of the streamwise evolution of Görtler vortices, i.e. the difference between the most downstream amplified mode and the optimal inlet conditions, the strong sensitivity of the spatial gain to inlet conditions as well as the fast initial growth of the optimal perturbations near the inlet station, may be essentially ascribed to the non-normality of the propagator $P_{[x,x_0]}$.

Much attention has recently been given to *temporal* transient amplification mechanisms in *stable* flows (see, for instance, Trefethen et al. [23] for a review). Our goal here is rather different: we want to investigate the effect of the non-normality of the propagator on the *spatial* dynamics in an *unstable* system. To illustrate this point let us examine the simple linear two-dimensional "toy" system

$$\frac{\mathrm{d}\mathbf{s}}{\mathrm{d}x} = \mathbf{A}\mathbf{s}, \tag{30}$$

with

$$\mathbf{A} = \begin{bmatrix} \mu_1 & \gamma \\ 0 & \mu_2 \end{bmatrix}, \tag{31}$$

which is analogous to the models considered for instance by Trefethen et al. [23], Schmid and Henningson [21], and Farrel and Ioannou [7]. Since spatial evolution is modelled rather than temporal dynamics, time t has been simply replaced by "streamwise" distance x. The most fundamental difference with the above analyses is that we consider an unstable system with $\mu_1 > 0$.

The solution of Equation (30) is formally given by

$$\mathbf{s}_{[x]} = \mathbf{P}_{[x,x_0]}\mathbf{s}_{[x_0]} \tag{32}$$

when an "inlet" condition $s_{[x_0]}$ is applied at x_0. In the autonomous case, i.e. when (μ_1, μ_2, γ) do not depend on x, the propagator is given by

$$\mathbf{P}_{[x,x_0]} = e^{\mathbf{A}(x-x_0)} \equiv \begin{bmatrix} e^{\mu_1(x-x_0)} & \frac{\gamma\left(e^{\mu_2(x-x_0)} - e^{\mu_1(x-x_0)}\right)}{\mu_2-\mu_1} \\ 0 & e^{\mu_2(x-x_0)} \end{bmatrix}. \tag{33}$$

Let us first summarize the properties of the propagator (33): its eigenvalues are $e^{\mu_i(x-x_0)}$, $i = 1, 2$. We assume that $\mu_1 > 0$ and $\mu_2 < 0$ so that the first (second) eigenvalue of $P_{[x,x_0]}$ is greater (less) than unity in absolute value for all $x > x_0$, thus implying instability (stability) of the corresponding mode. The associated eigenvectors are $\boldsymbol{\psi}^{(1)} = \{1, 0\}$ (spatially amplified), and $\boldsymbol{\psi}^{(2)} = \{\gamma, (\mu_2 - \mu_1)\}$ (spatially decaying). When $\gamma = 0$, the eigenvectors of $\mathbf{P}_{[x,x_0]}$ are orthogonal and $\mathbf{P}_{[x,x_0]}$ is said to be a *normal operator* [23]. When $\gamma \neq 0$, they are not orthogonal and $\mathbf{P}_{[x,x_0]}$ is said to be *non-normal*. The adjoint of the propagator with respect to the Euclidean norm is obtained by simply transposing matrix (33). The adjoint eigenmodes are $\boldsymbol{\psi}^{(1)^*} = \{(\mu_2 - \mu_1), -\gamma\}$ and $\boldsymbol{\psi}^{(2)^*} = \{0, 1\}$.

When $\gamma \neq 0$, the eigenvectors of the adjoint operator are seen not to coincide with the eigenvectors of the original operator. Thus, the vector of (Euclidean) norm unity that has the largest component along a given eigenvector, when expanded on the basis of eigenvectors, is not this eigenvector but the corresponding adjoint eigenvector. As a consequence, in the stable case, non-normal propagators, in contradistinction with normal ones, may exhibit amplified transients in spite of the fact that all the eigenvalues of $\mathbf{P}_{[x,x_0]}$ are of absolute value less than unity. Most of the interest has so far been focused on counter-intuitive transient amplifications in stable fluid systems such as Couette and Poiseuille flows. In the unstable case, non-normality of the propagator may still induce large initial transient growths. The feature we wish to illustrate and emphasize is that non-normality may be associated with extra gain at large time or "streamwise" distance, i.e. *a gain larger than the integrated growth associated with the leading eigenvalue.*

The effect of a rescaling of the state variables is now examined in the context of the problem (30), (31). Let $\hat{s}_1 = s_1$, $\hat{s}_2 = \mathrm{Re}^{-1/2} s_2$ denote the "physical" state vector where s_1 is the analogue of the u-velocity component and s_2 the analogue of the v-velocity component. The "physical" and the rescaled "boundary-layer" state vectors are related through a rescaling matrix $\mathbf{R}$ via the expression

$$\hat{\mathbf{s}}_{[x]} = \mathbf{R}\mathbf{s}_{[x]}, \quad \mathbf{R} = \begin{bmatrix} 1 & 0 \\ 0 & \mathrm{Re}^{-1/2} \end{bmatrix}. \tag{34}$$

The expression of the propagator in "physical" variables can then be readily obtained by substitution of (34) into (32) to obtain

$$\hat{\mathbf{s}}_{[x]} = \hat{\mathbf{P}}_{[x,x_0]}\hat{\mathbf{s}}_{[x_0]}, \tag{35}$$

where

$$\hat{\mathbf{P}}_{[x,x_0]} = \mathbf{R}^{-1}\mathbf{P}_{[x,x_0]}\mathbf{R} \equiv \begin{bmatrix} e^{\mu_1(x-x_0)} & \frac{\mathrm{Re}^{1/2}\gamma\left(e^{\mu_2(x-x_0)} - e^{\mu_1(x-x_0)}\right)}{\mu_2-\mu_1} \\ 0 & e^{\mu_2(x-x_0)} \end{bmatrix}. \tag{36}$$

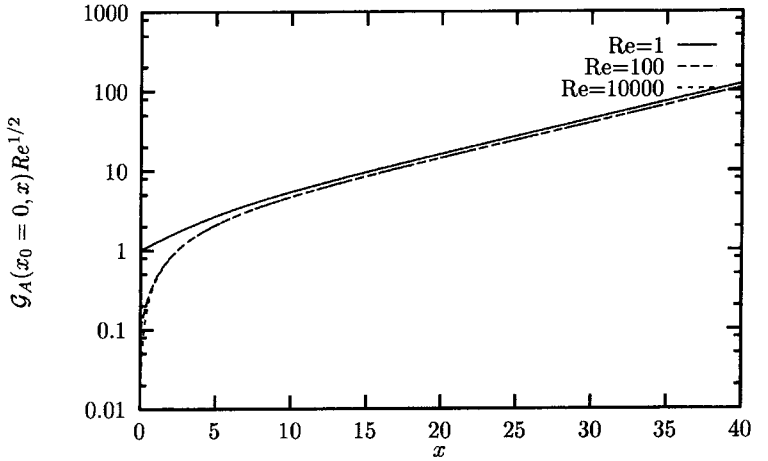

Figure 7. Maximum gain curves $\mathcal{G}_A(x_0, x)/\mathrm{Re}^{1/2}$ of "toy" system (30), (31), with $\mu_1 = 1/10$, $\mu_2 = -1/10$, $\gamma = -3$, for Reynolds numbers Re = 1, 10^2, 10^4.

When the Reynolds number is finite the **R** matrix is non-singular. In this case it can be easily seen that the propagators $\mathbf{P}_{[x,x_0]}$ in "boundary layer" variables and $\hat{\mathbf{P}}_{[x,x_0]}$ in "physical" variables have the same eigenvalues. The effect of rescaling on the propagator is merely to rescale γ via an equivalent $\hat{\gamma} = \gamma \mathrm{Re}^{1/2}$, i.e. to increase the non-normality of the propagator.

The "physical" energy is given by the square of the (Euclidean) norm of $\hat{\mathbf{s}}_{[x]}$. The analogue of the g_A gain is based on the norm pertaining to the rescaled state vector $\hat{\mathbf{s}}_{[x]}$

$$g_A^2(x_0, \hat{\mathbf{s}}_{[x_0]}, x) = \frac{\|\hat{\mathbf{s}}_{[x]}\|^2}{\|\hat{\mathbf{s}}_{[x_0]}\|^2} = \frac{\hat{s}^2_{[x],1} + \hat{s}^2_{[x],2}}{\hat{s}^2_{[x_0],1} + \hat{s}^2_{[x_0],2}} = \frac{s^2_{[x],1} + \mathrm{Re}^{-1} s^2_{[x],2}}{s^2_{[x_0],1} + \mathrm{Re}^{-1} s^2_{[x_0],2}}. \tag{37}$$

As the Reynolds number increases, an increase of non-normal effects is to be expected. In Figure 7 the maximum spatial gain curves $\mathcal{G}_A/\mathrm{Re}^{1/2}$ are displayed for Re = 1, Re = 100 and Re = 10000. For Re = 1 the g_A gain coincides with the gain of the propagator $\mathbf{P}_{[x,x_0]}$ in the "boundary layer" variables. The other two curves almost coincide except for the very upstream portion, since for $x = 0$ they start with the value $1/\mathrm{Re}^{1/2}$. For large Reynolds numbers (in our example Re > 100) the rescaled maximum spatial gain curves become almost Reynolds number independent as yet observed by Andersson et al. [2] and the limiting value is given by the g_L gain. The initial growth is seen to be very strong as observed in Figure 4 for the Görtler system. The optimal inlet condition for large optimization stations x is given by the adjoint eigenvector $\hat{\boldsymbol{\psi}}^{(1)*} = \{(\mu_2 - \mu_1), -\gamma \mathrm{Re}^{1/2}\}$ while the "optimal response" is proportional to $\hat{\boldsymbol{\psi}}^{(1)} = \{1, 0\}$. For large Reynolds numbers one recovers the result that the optimal inlet condition is nearly orthogonal to the optimal response. This is exactly what happens when one uses Luchini's gain

in which the optimal inlet (with $u_0 = 0$) is orthogonal to the optimal ouput (with $v = 0$ and $w = 0$) i.e. $\int_0^\infty uu_0 + \mathrm{Re}^{-1}(vv_0 + ww_0)\,\mathrm{d}y = 0$.

6. Discussion and Conclusions

A flexible numerical optimization technique has been used to determine the x–x_0 optimal inlet conditions which, applied at a given upstream inlet location x_0, maximize the amplitude of Görtler vortices at some downstream location x. In the linear approximation, perturbation velocity profiles at a given station x are related to those imposed at the inlet x_0 through the *spatial propagator* of the system. A numerical approximation to the spatial propagator has been constructed by using a set of numerical simulations of the downstream response associated with a complete set of linearly independent inlet conditions. The parabolic system of equations governing the spatial evolution of Görtler vortices has been solved numerically with the downstream marching technique proposed by Hall [12].

In the present analysis the inlet station is taken at a finite distance from the leading edge of the curved plate, where the boundary layer thickness is finite, and the maximum spatial growth is computed. Even if the curvature starts at the leading edge, perturbations may be introduced in the boundary layer by many different receptivity mechanisms, not all known, and all not active just at the leading edge. Therefore, the maximum spatial growth computed here decouples the leading edge receptivity from the subsequent evolution of the perturbation and gives a global upper bound for spatial growth between two spatial stations, no matter how the disturbances entered the boundary layer upstream. The present analysis has shown that close to the leading edge Görtler vortices are still receptive to free-stream perturbations since the optimal inlet condition there has a large amplitude outside the boundary layer. When the inlet station is selected to be further downstream, the optimal inlet perturbation is entirely localized inside the boundary layer, indicating that the amplification is not due to receptivity but to the instability of the boundary layer. If one is interested in delaying transition to turbulence by optimal or robust control it is essential to account for the possibility of transient growth and to evaluate the norm of the open loop transfer functions between inlet disturbances and the selected performance measures [3]. These transfer functions can be obtained from an optimization performed on the spatial propagator of the system.

Optimal perturbations have been determined by suitably postprocessing the computed propagator. We have chosen the gain definition proposed by Luchini [14] which consists, for infinite Reynolds numbers, in the ratio between the outlet and inlet perturbation energy density. The optimal inlet perturbations are periodic streamwise counter-rotating vortex pairs that generate streamwise streaks further downstream. The optimal inlet condition as well as the corresponding downstream response display a strong qualitative resemblance with the optimal perturbations found by Luchini [14] and Andersson et al. [2] in the flat plate case. The flat plate boundary layer analyzed by these authors was stable in the streamwise range which

they considered, and the observed streamwise growth was necessarily of a transient nature, while the concave wall boundary layer considered here is unstable and perturbations keep growing downstream. Furthermore, the optimal perturbations calculated by Luchini and Andersson et al. are given at the leading edge of the plate, where the boundary layer has zero thickness, while the optimal perturbations considered here are given downstream of the leading edge, where the boundary layer has a finite thickness. It has been verified that as the inlet station is moved upstream, the distribution of optimal inlet conditions moves outside the boundary layer into the free-stream, and it seems to converge to a non-singular perturbation distribution at the leading edge $x_0 = 0$. This result indicates that, for a fixed spanwise wavelength, optimal perturbations of the Görtler vortices do not scale with the boundary layer thickness. When inlet perturbations are applied sufficiently far upstream, the optimal perturbations are located outside the boundary layer. Downstream of the leading edge, the boundary layer is still strongly receptive to free-stream disturbances. Thus, not only leading edge receptivity per se but also receptivity to free-stream disturbances all along the boundary layer should be taken into account.

The total gain strongly depends on the selected inlet condition so that the prediction of transition stations based on critical gains, e.g. the widely used e^N-method, is expected to be very sensitive to different upstream forcings. Furthermore, the optimal inlet conditions strongly differ from the most amplified mode that emerges far downstream. Even if the non-parallelism of the base flow is known to be an essential ingredient in the spatial dynamics of the Görtler instability and this effect is taken into consideration to determine the spatial propagator, non-parallelism alone does not necessarily account for the spatial evolution of Görtler vortices. The non-normality of the associated spatial propagator is suspected to give rise to long spatial transients that are then sustained downstream by the Görtler instability, as illustrated on a simple "toy" dynamical system. Several qualitative features of the Görtler flow are reproduced by the "toy" system and may be attributed to the non-normality of the spatial propagator. In particular the strong sensitivity of the perturbation evolution, the large additional gain generated by optimal perturbations, when compared to local eigenmode perturbations, and the wide differences between optimal inlet conditions and the far downstream response, strongly support an interpretation of these effects in terms of non-normality considerations.

Appendix A

Let D denote partial differentiation with respect to y. The operators appearing in Equations (8) are then defined as follows:

$$M^{(uu)} = -U, \tag{38}$$

$$M^{(uv)} = 0, \tag{39}$$

$$M^{(vu)} = 2\left(\frac{\partial^2 U}{\partial x \partial y} + \frac{\partial U}{\partial y} D\right), \tag{40}$$

$$M^{(vv)} = \frac{\partial^2 U}{\partial y^2} + U(\beta^2 - D^2), \tag{41}$$

$$L^{(uu)} = (D^2 - \beta^2) - \frac{\partial U}{\partial x}, \tag{42}$$

$$L^{(uv)} = -VD - \frac{\partial U}{\partial y}, \tag{43}$$

$$L^{(vu)} = \frac{\partial V}{\partial x}(D^2 + \beta^2) + \frac{\partial^3 U}{\partial x^2 \partial y} + 2G^2\beta^2, \tag{44}$$

$$L^{(vv)} = \left(\beta^2 - D^2\right)^2 + \left(\beta^2 - D^2\right)\frac{\partial V}{\partial y} + \frac{\partial^3 U}{\partial x \partial^2 y} - VD^3 + \frac{\partial^2 U}{\partial x \partial y} D + \beta^2 D. \tag{45}$$

Associated boundary conditions read:

$$\begin{aligned} &u(x,0) = 0, \quad u(x,\infty) = 0; \\ &v(x,0) = 0, \quad v(x,\infty) = 0; \\ &Dv(x,0) = 0, \quad Dv(x,\infty) = 0. \end{aligned} \tag{46}$$

Appendix B

The objective of this appendix is to discretize the integrals used to define the gains in Equations (16) and (17). First of all, a conversion from the normal physical coordinate y to the normal boundary layer coordinate η is necessary because the equations have been discretized in η. For instance, the u^2-integral gives

$$\int_0^\infty u^2 \, \mathrm{d}y = 2x^{1/2} \int_0^\infty u^2 \, \mathrm{d}\eta. \tag{47}$$

Using a simple trapezoidal integration rule and taking into account boundary conditions (46), the integral can be further reduced to

$$\int_0^\infty u^2 \, \mathrm{d}\eta = \Delta\eta \sum_{j=1}^{N_\eta - 1} u^2(x, \eta_j) = \Delta\eta \, \mathbf{u}_{[x]}^T \mathbf{u}_{[x]}, \tag{48}$$

so that one obtains

$$\int_0^\infty u^2 \, \mathrm{d}y = 2x^{1/2} \Delta\eta \, \mathbf{u}_{[x]}^T \mathbf{u}_{[x]}. \tag{49}$$

In a similar way it is found that

$$\int_0^\infty v^2 \, dy = 2x^{1/2} \Delta\eta \, \mathbf{v}_{[x]}^T \mathbf{v}_{[x]}, \quad \int_0^\infty w^2 \, dy = 2x^{1/2} \Delta\eta \, \mathbf{w}_{[x]}^T \mathbf{w}_{[x]}. \tag{50}$$

By substitution into Equations (16) and (17) one finally obtains:

$$g_L^2(x_0, \mathbf{v}_{[x_0]}, x)/\mathrm{Re} = \left(\frac{x}{x_0}\right)^{1/2} \frac{\mathbf{u}_{[x]}^T \mathbf{u}_{[x]}}{\mathbf{v}_{[x_0]}^T \mathbf{v}_{[x_0]} + \mathbf{w}_{[x_0]}^T \mathbf{w}_{[x_0]}}. \tag{51}$$

Appendix C

In this appendix we compare the computational cost of the direct (D) "discrete propagator approach", used here, to the iterative (I) "direct-adjoint approach" used by Andersson et al. [2] and Luchini [14].

For the (D) approach we assume that a finite difference code is used in order to march an inlet condition downstream and that this code requires kN_η operations to advance the solution by one spatial increment Δx. The first step consists in the computation of the propagator at each streamwise station. As the number of independent variables is 2, this requires the downstream integration of $2N_\eta$ upstream conditions and thus $2kN_\eta^2 N_x$ operations. Assume then that a power iteration method is used in order to compute the optimal perturbations and growth. The operator $\mathbf{P}_{[x_k,x_0]}^T \mathbf{P}_{[x_k,x_0]}$ is applied at each iteration. If c is the number of iterations required to converge the power iterations, as each iteration requires the evaluation of the propagator and the adjoint propagator on a state vector, $2c(2N_\eta)^2$ operations are needed for each optimization. If the optimals are evaluated at streamwise stations separated by $p\Delta x$ (i.e. in N_x/p points), the total number of operations for the optimization process is then $8cN_\eta^2 N_x/p$. Globally the (D) approach will thus require $(2k + 8c/p)N_\eta^2 N_x$ operations.

In the (I) approach a power iteration method is also used. However, instead of computing the propagator and its adjoint, one marches downstream the direct equations (instead of applying $\mathbf{P}_{[x_k,x_0]}$) and marches upstream the adjoint equations (instead of applying $\mathbf{P}_{[x_k,x_0]}^T$) at each iteration. We assume that the same finite difference code as for the (D) approach is used to perform the direct integration, and that a similar code is used for the adjoint upstream marching. Of course, the number c of iterations required in order to converge the iterations is the same as for the (D) approach. In order to compute the optimal perturbations and growth at the $x_j = j\Delta x$ streamwise station, the total number of operations will thus be $2ckjN_\eta$. The number of operations needed by the (I) approach to evaluate the optimal perturbations and the optimal growth at streamwise stations separated by $p\Delta x$ is $2ckN_\eta \sum_{j=1}^{N_x/p} pj = (ck/p)N_\eta N_x(N_x + p)$.

The ratio of the operations required by the (D) to those required by the (I) approach is therefore

$$\frac{(2k + 8c/p)N_\eta}{(ck/p)(N_x + p)}. \tag{52}$$

From Equation (52) one may observe, for instance, that the (D) approach requires more operations than the (I) approach when the optimization stations are not far from the inlet ($N_x \ll N_\eta$) and/or when a small number of optimization stations is analyzed [$p/N_x = O(1)$]. However, when many optimization stations are analyzed ($p/N_x \ll 1$) and when they are not too close to the inlet station ($N_x \gg N_\eta$), the (D) approach may, unintuitively, require *less* operations than the (I) approach. For instance, in the case analyzed in this article the average power iteration number was $c = 4$, the constant k was of the order of 5 and $p = 1$. In a typical simulation $N_\eta = 200$ and $N_x = 2200$. With this set of parameters, the ratio of operations used here, compared to the number of operations required by a direct/adjoint approach is, according to Equation (52), about 1/5. If we had decided to evaluate the optimal growths and perturbation every 10 spatial steps (i.e. $p = 10$) the ratio would have been about 3/5.

Acknowledgment

The computational facilities of the Institut du Développement et des Ressources en Informatique (IDRIS/CNRS) under grant 970761/CP6 are gratefully acknowledged.

References

1. Anderson, E., Bai, Z., Bishof, C., Demmel, J., Dongarra, J., Croz, J.D., Greenbaum, A., Hammarling, S., Kenney, A.M., Ostuchov, S. and Sorensen, D., *LAPACK Users' Guide, Release 1.0.* SIAM, Philadelphia, PA (1992).
2. Andersson, P., Berggren, M. and Henningson, D., Optimal disturbances and bypass transition in boundary layers. *Phys. Fluids* **11**(1) (1999) 134–150.
3. Bewley, T.R. and Liu, S., Optimal and robust control and estimation of linear paths to transition. *J. Fluid Mech.* **365** (1998) 305–349.
4. Bottaro, A. and Luchini, P., Görtler vortices: Are they amenable to local eigenvalue analysis? *Eur. J. Mech. B* **18** (1999) 47–65.
5. Coddington, E.A. and Levinson, N., *Theory of Ordinary Differential Equations.* McGraw-Hill, New York (1955).
6. Day, H.P., Herbert, T. and Saric, W.S., Comparing local and marching analyses of Görtler instability. *AIAA J.* **28**(6) (1990) 1010–1015.
7. Farrell, B.F. and Ioannou, P.J., Generalized stability theory. Part I: Autonomous operators. Part II: Nonautonomous operators. *J. Atmos. Sci.* **53** (1996) 2025–2053.
8. Floryan, J.M., On the Görtler instability of boundary layers. *Prog. Aerosp. Sci.* **28** (1991) 235–271.
9. Floryan, J.M. and Saric, W.S., Stability of Görtler vortices in boundary layers. *AIAA J.* **20**(3) (1982) 316–324.

10. Görtler, H., Instabilität laminarer Grenzschichten an konkaven Wänden gegenüber gevissen dreidimensionalen Störungen. *ZAMM* **21** (1941) 250–252.
11. Hall, P., Taylor–Görtler vortices in fully developed or boundary layer flows: Linear theory. *J. Fluid Mech.* **124** (1982) 475–494.
12. Hall, P., The linear development of Görtler vortices in growing boundary layers. *J. Fluid Mech.* **130** (1983) 41–58.
13. Hall, P., Görtler vortices in growing boundary layers: The leading edge receptivity problem, linear growth and nonlinear breakdown stage. *Mathematika* **37** (1990) 155–189.
14. Luchini, P., Reynolds-number independent instability of the boundary layer over a flat surface. Part 2: Optimal perturbations. *J. Fluid Mech.* **404** (2000) 289–309.
15. Luchini, P. and Bottaro, A., Görtler vortices: A backward-in-time approach to the receptivity problem. *J. Fluid Mech.* **363** (1998) 1–23.
16. Lundbladh, A., Schmid, P.J., Berlin, S. and Henningson, D.S., Simulation of bypass transition in spatially evolving flows. In: *Proceedings of the AGARD Symposium on Application of Direct Large Eddy Simulation to Transition and Turbulence*. AGARD CP-551 (1994) pp. 18–21.
17. Park, D.S. and Huerre, P., Primary and secondary instabilities of the asymptotic suction boundary layer on a curved plate. *J. Fluid Mech.* **283** (1995) 249–272.
18. Press, W.H., Flannery, B.P., Teukolsky, S.A. and Vetterling, W.T., *Numerical Recipes*. Cambridge University Press, Cambridge, U.K. (1986).
19. Saric, W.S., Görtler vortices. *Annu. Rev. Fluid Mech.* **26** (1994) 379–409.
20. Schlichting, H., *Boundary-Layer Theory*. McGraw-Hill, New York (1979).
21. Schmid, P. and Henningson, D.S., Optimal energy density growth in Hagen–Poiseuille flow. *J. Fluid Mech.* **277** (1994) 197–225.
22. Swearingen, J.D. and Blackwelder, R.F., The growth and breakdown of streamwise vortices in the presence of a wall. *J. Fluid Mech.* **182** (1987) 255–290.
23. Trefethen, L.N., Trefethen, A.E., Reddy, S.C. and Driscoll, T.A., Hydrodynamic stability without eigenvalues. *Science* **261** (1993) 578–584.
24. Wilkinson, J.H., *The Algebraic Eigenvalue Problem*. Clarendon Press, Oxford (1965).